An analytical validation for the attenuation of lateral propagating light in sea ice

ZHAO Jinping[1]*, LI Tao[1], EHN Jens[2], BARBER David[2]

[1] Physical Oceanography Laboratory, Ocean University of China, Qingdao 266100, China
[2] Centre for Earth Observation Science, University of Manitoba, Winnipeg R3T 2N2, Manitoba, Canada

Abstract

The attenuation of lateral propagating light (LPL) in sea ice was measured using an artificial light source in the Canadian Arctic during the 2007/2008 winter. The apparent attenuation coefficient $\mu(\lambda)$ for lateral propagating light was obtained from the measured logarithmic relative variation rate. In this study an analytical solution based on the strict optical theories is developed to validate the measured result. There is a good consistency between theoretical solution and measured data, by which a quite simple but very rigorous relationship among the light source, measurement geometry, and measured irradiance is established. The attenuation coefficients acquired by measurement and theory are the diffusion attenuation as an apparent optical property of ice, independent of the light source and shining condition. The attenuation ability of sea ice should be caused by the microstructure of sea ice, such as crystal size, ice density, brine volume, air inclusion, etc. It also includes the leak from both interfaces by directional scattering. It is verified that the measuring approach is operational and accurate to measure the attenuation of the LPL. The solution from this study did not tell the connection among the extinction and the inclusions of sea ice theoretically because of insufficient understanding.

Key words: Arctic, sea ice, lateral propagating light, optical attenuation coefficient, artificial light, analytical solution

---

1 Introduction

The presence of sea ice significantly influences the regional climate and amplifies the global warming in the Arctic (Holland et al., 2006). It is also a sensitive indicator of climatic changes. Presently the sea ice in the Arctic Ocean is undergoing a rapid decrease in extent, thickness and concentration (Rothrock et al., 1999; Parkinson, 1999; Tucker et al., 2001; Lindsay and Zhang, 2005), with a record minimum ice extent reached in 2012 (Parkinson and Comiso, 2013; Zhang et al., 2013). In particular, the once dominant perennial sea ice cover has dramatically decreased with a consequent transition of the Arctic Ocean towards a seasonal sea ice zone. With this rate, a seasonally ice free Arctic is expected before 2030 as estimated by some researchers (e.g., Barber and Massom, 2007).

The interactions of solar radiation with the sea ice cover is of key importance for the understanding of the currents ice trends and consequences to, e.g., biological productivity in the Arctic Ocean (Mundy et al., 2009; Arrigo et al., 2012). Radiative transfer in the young sea ice is much different from that in multiyear ice in the similar solar insolation condition (Maykut and Grenfell, 1975). An effective way to understand the attenuation of solar radiation inside sea ice is to measure the apparent optical properties including diffuse attenuation, albedo and transmission by optical instruments. The light attenuation in sea ice is governed by its microstructure, which includes properties such as ice crystal size, and brine pockets and air bubbles imbedded within the sea ice matrix and that effectively scatter light (REF). Further attenuation is caused by absorption of the ice and brine themselves, and by impurities within the sea ice, which include various particulate and dissolved materials that mainly absorb radiation (e.g., Ehn et al. 2008a, b). The attenuation of solar radiation with depth is thus a result of both absorption and scattering, which are so called inherent optical properties and typically either determined through laboratory experiments (Grenfell and Perovich, 1981) or inferred from field observations of apparent optical properties, which for example include diffuse attenuation, albedo and transmittance (e.g., Ehn et al., 2008b). The largest part of the diffuse attenuation of solar radiation in sea ice is due to scattering, which is controlled by the volume fractions, number densities and shapes of brine and air inclusions (Schoonmaker et al., 1989; Light et al., 2004). Two fundamental characteristics of scattering are measured by laboratory experiments: the scattering phase function and scattering coefficient (Voss and Schoonmaker, 1992; Gilbert and Schoonmaker, 1990).

The main *in situ* optical measurements for sea ice are focused on the upwelling and downwelling planar irradiances, i.e., the vertically propagating radiation components. The downwelling irradiance is related to the transmission of the solar energy flux through sea ice, which is important to both sea ice and underlying seawater for the energy budget (Zhao et al., 2009; Zhao and Li, 2010). The upward propagating light is

formed by the backscatter of light from the surface, the interior of the sea ice and from the underlying water column, and play a crucial role in the building of the albedo of the surface, which is of key importance for climate studies and remote sensing (Perovich et al., 1998).

Due to the horizontal nature of ice formation on the ocean surface and the source of illumination being almost equally distributed from above, the main interest is radiation propagation in the vertical direction, however, the diffusion of radiation in a scattering medium occurs in all directions. For example, the blue, green or white color of thick multi-year ice, particularly well seen from portions located beneath the seawater surface, is a good illustration of the presence of horizontal component of light propagation, which we hereinafter refer to as laterally propagating light (LPL). The measurement of attenuation for LPL in an undeformed thermodynamically grown ice sheet is not meaningful in natural conditions because the light field is essentially uniform in the horizontal dimension, while attenuating rapidly with distance in the vertical dimension. The light field in sea ice becomes increasingly downward directed in sea ice because the horizontally propagating component is preferentially attenuated due to a longer pathlength of travel. Futhermore, the attenuation of light in sea ice is anisotropic; the vertical component perpendicular to the air-ice interface is depth-dependent because sea ice essentially a vertically layered medium (Perovich, 1996) and horizontally the attenuation is different from that in the vertical due to the anisotropic crystal structure of sea ice with vertically elongated scattering inclusions (Haines et al., 1997; Trodahl et al., 1989). To date, we have little knowledge about LPL attenuation and diffusion, and the structural-optical properties that control them, particularly in the thinner and younger sea ice types.

Studies of directional propagating light in natural sea ice are rare (Pegau and Zandveld, 2000). Buckley and Trodahl (1987a, b), Trodahl et al. (1987) and Haines et al. (1997) presented their experiments on the Antarctic sea ice by a novel measuring geometry and a quartz-halogen lamp to measure the anisotropic scattering of light, the scattering length, their correlation with salinity, and the different optical properties in surface, bulk and ice algae layers. Maffione et al. (1998) used a novel method to measure the beam spread function laterally in sea ice and described the radiative transfer by the photon diffusion theory. Zhao et al. (2010) designed a field experiment using a flat artificial light source on the surface (facing downwards) and by burying a radiometer into the ice and pointing it horizontally to measure LPL on winter sea ice in the Canadian Arctic during the winter of 2007–2008. The light source was moved on the surface to create horizontal distance to the radiometer. Foreoptics was mounted on the instrument to reduce the field of view for the measurement to 5.8°. The variation in intensity of the LPL was measured with the lamp moved to different locations. The apparent attenuation coefficient $\mu(\lambda)$ for LPL was obtained from the measured logarithmic relative variation rate. With the exception of blue and red light, the attenuation coefficient changed little with wavelength, but changed considerably with salinity: the greater the salinity, the greater the attenuation coefficient through influences on volume of brine inclusions. The observed LPL attenuation coefficient was much larger than that of vertical propagation light and could not be fully explained by anisotropic scattering properties alone.

Although the measured LPL attenuation coefficient increased our understanding of how light is attenuated parallel to the air-ice interface by sea ice, Zhao et al. (2010) still lacked

a physical comprehension on the background of the attenuation coefficient. The motivation for this study is to establish the relationship between physical properties of the ice and light attenuation in young sea ice. In this study, a physical framework is established by considering the connection among the light source, radiation transfer, and measuring geometry. Based on strict optical theories the radiative transfer process is modeled and an analytical solution is acquired successfully. The result here will benefit energy balance studies in sea ice.

2 Field measurements for laterally propagating light (LPL)

The measured lateral attenuation in the sea ice is based on an experiment in winter Arctic (Zhao et al., 2010), from 11 November 2007 to 31 January 2008 in the Amundsen Gulf, southern Beaufort Sea supported by the Canadian research icebreaker *Amundsen* and by the Circumpolar Flaw Lead (CFL) system study project (Fig. 1). During the experiment, all the sea ice was
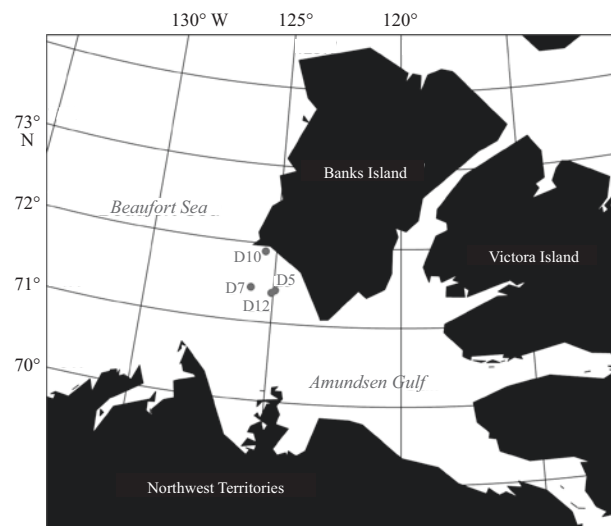
Fig. 1. Field measurement stations for lateral propagating light in Amundsen Gulf in winter from November 11 of 2007 to January 31 of 2008.

first-year ice with a thickness between 0.5 and 1.2 m. A custom-designed artificial light source consisting of ten fluorescent bulbs within an area of 1.3 m by 0.96 m was constructed to form a rectangular plane lamp. The radiative properties of the lamp were described in Zhao et al. (2008). The spectroradiometer used was the Profiling Reflectance and Radiometer System (PRR-810) from Biospherical Inc. (USA) equipped to measure eighteen wavebands from 313 to 870 nm. The light source contained all the wavelengths within 313–870 nm, though the spectral distribution of the lamp is different from that of the sun. A fore-optic was attached to the PRR-810 to reduce the field-of-view (FOV) from hemispheric to 5.8° in order to collect the scattering light from a very small solid angle as adopted by Hanesiak et al. (2001). A trench was cut in the sea ice and the sidewall was polished to remove any matter that could increase scattering. The PRR-810 was then positioned in the trench horizontally and was buried by ice crumb at different depths. The top surface of the trench was smoothed out to facilitate the movement of the lamp on the surface (Fig. 2). The measurement by a moving lamp is equivalent to the measurement using a fixed lamp and a moving instrument assuming a horizontally homogeneous sea
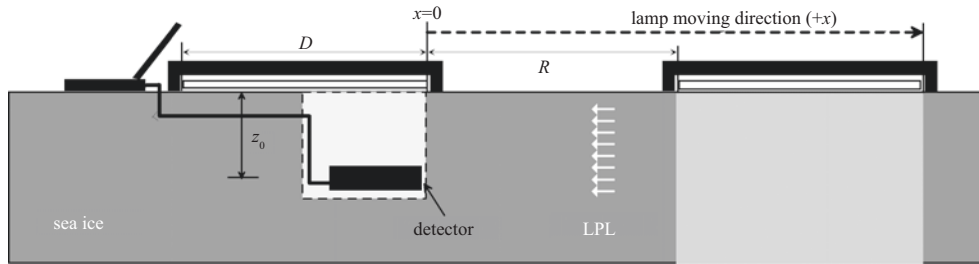
Fig. 2. Sketch of the experiment for attenuation of lateral propagating light where a trench is cut and an optical instrument is buried with the face of the detector to the right. The start position of the right edge of the lamp is at $x=0$, and it is moved to the right, $+x$ direction. The lateral propagating light (LPL) is transferred from the shining region to the left and reaches the detector. D is the length of the lamp. R is the value of the left edge of the lamp at x-coordinate, which is negative if the left edge of the lamp at the left of the detector. Data is obtained in real time with a computer.

ice cover. The lamp was positioned facing downwards with the shorter side (0.96 m) parallel to the direction of movement. The starting position of the lamp was with the centre of the lamp aligned with the axis of the PRR-810 and with the longer side of the lamp ($x=0$ in Fig. 2) aligned and parallel with the PRR-810's front face. The lamp was moved in increments by a marked rope and a crabstick until the measured radiation reached background levels. To standardize for surface illumination all LPL measurements had to be conducted in complete darkness (Fig. 3). The LPL was measured in 23 vertical levels at five stations (D5, D7, D10, D12 and D14). The measured results have been introduced by Zhao et al. (2010). Here we briefly introduce the main result of that experiment to facilitate the comparison with the analytical solution in this study.

When the lamp was moved to the front of the PRR-810 ($+x$ direction), the variation in irradiance $E(z, x, \lambda)$ with distance was as shown in Fig. 4. The irradiance was found to increase from

$x=0$ to a maximum at about 0.8 m as the lamp was gradually moved passed the plane of the PRR-810 sensor head. The irradiance then started to first decrease gradually until about the back edge of the lamp ($x=0.96$ m) after which a rapid decrease is seen as a gap opened up between the lamp and the PRR-810. As movement of the lamp altered the illumination conditions, the resulting curves in Fig. 4 reflect the transmission of lateral propagating light as a function of distance.

By dividing the irradiance of each record by the maximum irradiance $E_{ref}(z, x_0, \lambda)$ as a reference value, the relative variation of irradiance was obtained by

$$E(z, x, \lambda) / E_{ref}(z, x_0, \lambda). \tag{1}$$

Taking logarithm to the relative variation of irradiance (hereafter referred to as "logarithmic relative variation rate") and using the same data of Fig. 4, the result is shown in Fig. 5. When all of

Fig. 3. A photo taken for the field work in dark condition. Surrounding the lamp, there is a bright zone, which is the leaked scattering light out of the sea ice and caused stronger attenuation.
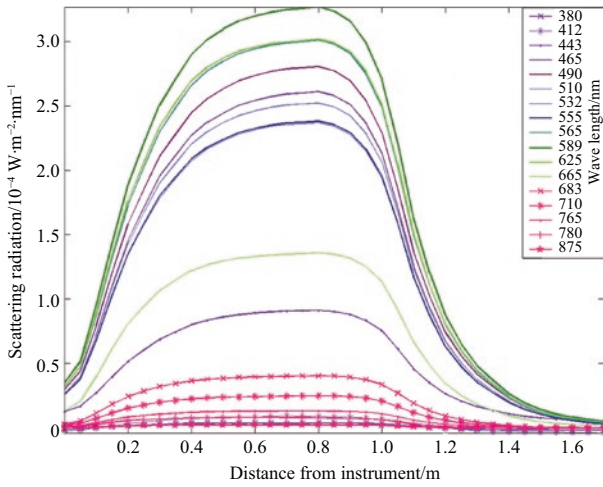
Fig. 4. Irradiance varied with the distance when the lamp moved at Sta. D5.
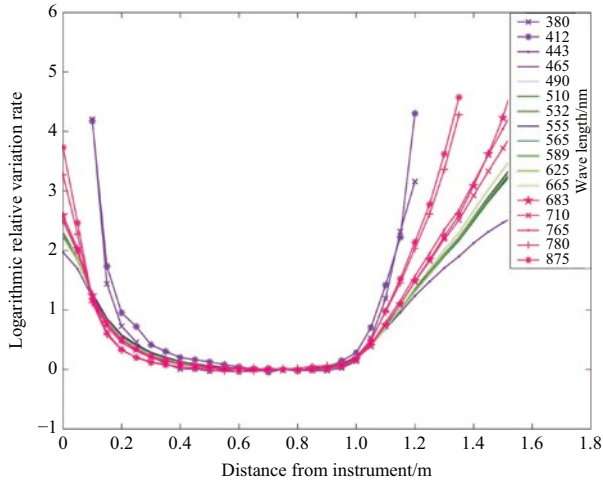
Fig. 5. Logarithmic relative variation of all wavelengths with the movement of lamp at Sta. D5. The nine wavelengths from 465 to 665 attenuate in the similar rate. The five red lines for red and infrared wavelengths and two violet lines for near violet wavelengths present greater attenuation. Light of 443 nm is obviously special with less linearity and less attenuation than the others.

the lamp was moved to the front and then beyond the PRR-810, as shown on Fig. 5 where the lamp movement distance exceeds 0.96 m, the logarithmic relative variation rate illustrated a linear extinction, hereafter referred to as the "linear portion". The formula appropriate for this linear portion is

$$\mu(\lambda)(x - x_0) + \ln\left[\frac{E(z, x, \lambda)}{E_{\text{ref}}(z, x_0, \lambda)}\right] = 0. \quad (2)$$

The slope of the straight line is the attenuation coefficient of LPL, $\mu(\lambda)$. The eight curves with the larger slopes, plotted in red and violet respectively, represent the red, infrared and near violet wavebands, which demonstrate stronger attenuation of the light at these wavelengths. The attenuation coefficients for the remaining nine wavebands (465–665 nm) are nearly the same magnitudes. This result is quite different from the spectral attenuation of direct incident light, which is wavelength-depen-

dent (Maykut and Grenfell, 1975).

The observed LPL attenuation coefficient is much larger than that of vertically propagating light. For example, the lateral attenuation coefficients at 490 nm are about 3.0–7.5 m⁻¹. However, the attenuation coefficient for vertically propagating light at the same wavelength is less than 1.0 m⁻¹ (Perovich et al., 1998). This result is quite similar with the experimentally-determined scattering coefficients of Haines et al. (1997), in which the attenuation in horizontal is 2–3 times larger than in the vertical direction. In the results of Zhao et al. (2010) only the linear portion when the lamp moved to the front of the instrument was published. Here, all the relative variation of irradiance (Fig. 4) and the logarithmic relative variation rate (Fig. 5) are displayed for validating.

The reason for stronger lateral attenuation is postulated that part of the LPL is scattered in vertical directions and leaked out of sea ice at the upper and lower interfaces. Figure 3 is a photo taken for the field work in dark conditions. Surrounding the lamp, there is a bright zone, which is the internally scattered light exiting out of the sea ice surface. The escaped light will be part of upwelling and downwelling radiation. The attenuation coefficient changed considerably with salinity, similar to the correlation between optical extinction and salinity found by Ehn et al. (2008) during their apparent optical properties measurements normal to the ice bottom interface.

The results of Zhao et al. (2010) created the measuring approach for the LPL, acquired the diffuse attenuation coefficient of LPL and found the relationship between the extinction and the salinity. But these results still need to be validated to ensure the measured attenuation coefficient is the property of the sea ice, independent of the measuring condition. Because the lamp used is with certain size, intensity and measuring geometry, one may question if the attenuation coefficient is not a lamp/measuring-dependent result. The best way to answer the question, as we will see in Section 3 is to establish a reliable physical relation to model the real measurement process.

3 Analytical solution for attenuation of lateral propagating light

The measured results by an artificial light source are inevitably related to the length and width of lamp, radiation intensity, and measurement geometry. If these conditions change will the result change accordingly? Is the measured lateral attenuation coefficient an optical feature of sea ice, or a measurement geometry-dependent result? The result in Zhao et al. (2010) did not answer these questions. Here we try to develop a physical framework to validate the observed results. If the measured and theoretical irradiance are consistent, then the measured attenuation coefficient will be validated and the measurement approach for LPL will be proven operational and acceptable.

Consider a dark environment with the only light coming from a lamp placed on the ice surface and shining downwards (Fig. 2). The origin of the z-coordinate was the upper surface of the sea ice, the depth of the PRR-810 was at z_0 from the surface, and the x-axis was the horizontal distance between the right margin of the lamp and PRR-810 (Fig. 2). Since the FOV of the PRR-810 fore-optic was 5.8°, the irradiance of LPL collected by the horizontally placed instrument was entirely scattered light. Consider a small volume dv anywhere within the ice cover which is illuminated by an irradiance $E_i(z, \lambda)$ arriving from the lamp. We may consider dv to approximate a point source. $E_i(z, \lambda)$ cause light scattering in dv which is radiated to the 4π space. The physical parameters relate satisfactorily to the following re-

lationship (Mobley, 1994)

$$\beta(\alpha,\delta,\lambda) = \frac{\mathrm{d}J_0(\alpha,\delta,\lambda)}{E_i(z,\lambda)\mathrm{d}v}, \tag{3}$$

where, α and δ are the zenith and azimuth angles and $\beta(\alpha, \delta, \lambda)$ is the volume scattering function ($\mathrm{m^{-1}\cdot sr^{-1}}$); $J_0(\alpha, \delta, \lambda)$ is the scattering radiant intensity from (α, δ) direction (W/sr), and (Mobley, 1994)

$$J_0(\alpha,\delta,\lambda) = \frac{\mathrm{d}\Phi(\alpha,\delta,\lambda)}{\mathrm{d}\Omega}, \tag{4}$$

where, $\Phi(\alpha, \delta, \lambda)$ is the scattering radiant flux of this point source $\mathrm{d}v$ from the (α, δ) direction. Ω is the solid angle to which the scattered radiation enters. If there is no absorption and scattering in the medium, the irradiance $E_s(z, \lambda)$ received by the instrument and caused by the point source in the vertical plane, $\mathrm{d}A$, at depth z down from the surface is (Mobley, 1994)

$$E_s(z,\lambda) = \frac{\mathrm{d}\Phi(\alpha,\delta,\lambda)}{\mathrm{d}A} = J_0(\alpha,\delta,\lambda)\frac{\mathrm{d}\Omega}{\mathrm{d}A}. \tag{5}$$

In the presence of absorption and scattering, the solution for radiative transfer is more complicated, and beam attenuation and multiple scattering have to be considered. Suppose the ice structure is horizontally-uniform and the spectral attenuation coefficient $c(\lambda)$ ($\mathrm{m^{-1}}$) is a wavelength dependent constant, the $J_0(\alpha, \delta, \lambda)$ in Eq. (5) will be replaced by $J(\alpha, \delta, \lambda)$,

$$J(\alpha,\delta,\lambda) = J_0(\alpha,\delta,\lambda)\exp\left[-c(\lambda)r\right], \tag{6}$$

where r is the distance from the point source to PRR-810. Equation (6) is a simplified expression of the complex attenuation and needs to be examined in terms of observed data.

Under the illumination of an artificial lamp, each small ice unit in the ice column can be considered as a point light source of LPL. In a spherical coordinate centered at the position of PRR-810 $(0, 0, z_0)$, θ is the angle of the incident light which is normal of the vertical area, $\mathrm{d}A$, φ is the azimuth angle, and r is the distance between the point light source and the PRR-810. In Eq. (5), $\mathrm{d}\Omega$ is a solid angle of the point source to a vertical plane $\mathrm{d}A$, the relation of both is $\mathrm{d}\Omega=\mathrm{d}A\cos\theta/r^2$. Then the irradiance from the single point source is

$$\mathrm{d}E_s(z_0,\lambda) = \frac{\mathrm{d}J(\alpha,\delta,\lambda)\cos\theta}{r^2}. \tag{7}$$

In atmospheric optics, Eq. (7) is used to calculate the illumination at a certain distance from the lamp and is known as Allard's Law (Dickson and Hales, 1963).

The irradiance caused by the ice column under the illumination of an artificial lamp is calculated by the integral of Eq. (7) for all ice units. Substituting Eqs (3) and (5) for Eq. (7), the irradiance becomes

$$E_s(z_0,\lambda) = \iiint_v \frac{\beta(\alpha,\delta,\lambda)E_i(z,\lambda)\cos\theta}{r^2}\exp\left[-c(\lambda)r\right]\mathrm{d}v, \tag{8}$$

where v is the volume of all radiation ice units. Because $\beta(\alpha, \delta, \lambda)$ is an unknown directional function correlated with sea ice features, the general solution of Eq. (8) therefore does not exist.

For a narrow FOV, however, only the scattered light along the horizontal plane can be collected, thus only the value of $\beta(\alpha, \delta,$

$\lambda)$ in (α_0, δ_0) direction needs to be considered. As it is a function of wavelength, and possibly related with depth in a horizontally homogeneous ice cover, the volume scattering function can be expressed as $\beta(z, \lambda)$. In Eq. (8), $E_i(z, \lambda)$ is the irradiance of incident light arriving at an ice unit and as a function of space and wavelength. The product of both can be combined as

$$F(z,\lambda) = \beta(z,\lambda)E_i(z,\lambda). \tag{9}$$

According to Eq. (3), the physical significance of $\beta(z, \lambda)\, E_i(z, \lambda)$ with the unit $\mathrm{W/m^{-3}\cdot sr^{-1}}$ is the scattered intensity from a unit volume, which is vertically varied and unknown. Because the FOV of the PRR-810 is quite small, $\theta\approx\theta_0$, $z\approx z_0$, and $r\approx x$ have a satisfactorily high accuracy. Integrating Eq. (8) to the narrow FOV for $\mathrm{d}v=r^2\cos\theta\mathrm{d}\theta\mathrm{d}\varphi\mathrm{d}r$, $E_s(z_0, \lambda)$, the measured irradiance for narrow FOV, becomes

$$E_S(z_0,\lambda) = F(z_0,\lambda)\int_0^{\theta_0}\cos^2\theta\int_{x_1/\cos\theta}^{x_2/\cos\theta}\exp[-c(\lambda)r]\int_0^{2\pi}\mathrm{d}\varphi\mathrm{d}r\mathrm{d}\theta,$$

or approximately

$$E_S(z_0,\lambda) = 2\pi F(z_0,\lambda)\int_0^{\theta_0}\cos^2\theta\mathrm{d}\theta\int_{x_1}^{x_2}\exp[-c(\lambda)x]\,\mathrm{d}x, \tag{10}$$

where x_1 and x_2 are the horizontal distances of two margins of the lamp to the sensor. Owing that θ_0 is very small, the approximating solution for Eq. (10) is

$$E_S(z_0,\lambda) = \frac{2\pi F(z_0,\lambda)\theta_0}{c(\lambda)}\left\{\exp[-c(\lambda)x_1] - \exp[-c(\lambda)x_2]\right\}, \tag{11}$$

Note that only the LPL from $(+x)$ direction is measured, and that the LPL from $(-x)$ direction should be omitted in Eq. (11). Assuming that the horizontal distance from the back margin of the lamp to original point is x, and the length of the lamp is D, and that the width of lamp and thickness of ice are suitable for a measurement with a narrow FOV, then

$$x_1 = \begin{cases} x & x \geqslant 0 \\ 0 & x < 0 \end{cases}, \tag{12a}$$

and

$$x_2 = x + D, \tag{12b}$$

and Eq. (11) can be expressed as

$$E_S(z_0,x,\lambda) = \frac{2\pi F(z_0,\lambda)\theta_0}{c(\lambda)}S_0[c(\lambda),x], \tag{13}$$

where

$$S_0[c(\lambda),x] = \begin{cases} \exp[-c(\lambda)x]\{1-\exp[-c(\lambda)D]\} & x \geqslant 0 \\ 1-\exp[-c(\lambda)(x+D)] & x < 0 \end{cases}. \tag{14}$$

From Eq. (14) it can be seen that the length of lamp D is important when the lamp is narrow, but if D is large, the value of $\{1-\exp[-c(\lambda)D]\}$ is very close to 1. It means that for a large enough D, the light from the lamp is similar to that from an infinite space, and the light entered into the instrument is nearly equal to that from only the edge of an infinitely large lamp.

In Eq. (13), as unknown $F(z_0, \lambda)$ and $c(\lambda)$ are included, the

$E_S(z_0, x, \lambda)$ is impossible to be acquired in this stage. If one want to acquire an analytical solution of $E_S(z_0, x, \lambda)$ by examination of the observed irradiance $E_i(z, \lambda)$, the $F(z_0, \lambda)$ related with the scattering property of sea ice caused by different inclusions must be thoroughly understood and expressed beforehand. Also, the attenuation coefficient $c(\lambda)$ should be accurately addressed in advance. The knowledge about the lateral scattering and attenuation are not yet sufficient to support such a theoretical study.

However, through the approach of calculating the logarithmic relative variation rate (Eq. 2), $F(z_0, \lambda)$, the one unknown factor in Eq. (13), can be eliminated. Choosing an irradiance at an arbitrary point, $x=x_0$, as a reference value following that of Eq. (2), the logarithmic relative variability rate for $x \geqslant 0$ becomes

$$-\ln\left[\frac{E_S(z_0, x, \lambda)}{E_{S\,\text{ref}}(z_0, x_0, \lambda)}\right] = -\ln\left[\frac{S_0[c(\lambda), x]}{S_0[c(\lambda), x_0]}\right] = c(\lambda)(x - x_0) \quad (x \geqslant 0). \quad (15)$$

Comparing of Eq. (15) with Eq. (2), if the analytical irradiance $E_S(z_0, x, \lambda)$ is a good modeling of the measured irradiance $E(z, x, \lambda)$, i.e.,

$$\ln\left[\frac{E(z, x, \lambda)}{E_{\text{ref}}(z, x_0, \lambda)}\right] = \ln\left[\frac{S_0[c(\lambda), x]}{S_0[c(\lambda), x_0]}\right], \quad (16)$$

then the theoretical attenuation coefficient $c(\lambda)$ should be equal to the measured attenuation coefficient $\mu(\lambda)$:

$$\mu(\lambda)(x - x_0) = c(\lambda)(x - x_0). \quad (17)$$

Although the analytical solution for irradiance of LPL is impossible to acquire and to compare with the measured ones, the logarithmic relative variation rates both from measured and analytical solution could be compared each other, as expected by Eq. (16). The right side of Eq. (16) only depends on two parameters, the attenuation coefficient $c(\lambda)$ and the length of the lamp D as shown in Eq. (14). As the $c(\lambda)$ is still unknown, both sides of Eq. (16) should be comparable only when the $c(\lambda)$ is replaced by observed $\mu(\lambda)$. The comparison result is plotted in Fig. 6.

The analytical solution of logarithmic relative variation rate (blue lines for right side of Eq. 16) and observed result (red lines for left of Eq. 16) at 490 nm at 0.05, 0.12, 0.22, and 0.32 m depth levels for Sta. D7 are shown in Fig. 6. Although the analytical solution is very simple and only composed of two connected curves, it is still very consistent with observed data. This means that the analytical solution reflects the real physical process of LPL attenuation well.

4. Discussion and conclusions

Equation (16) is an equality that will become valid when the measuring approach is adequate and the theoretical solution is correct. Since the analytical logarithmic relative variability rate depends on both $c(\lambda)$ estimated by the measured attenuation coefficient $\mu(\lambda)$ and the unchanged lamp length D, the analytical solution as expressed by Eqs (13) and (14) has nothing to adjust. If the lamp is placed wrongly, or wrong $\mu(\lambda)$ or wrong D are used, both the theoretical and the observational results will be inconsistent. So, the relationship of measured and modeled results is quite simple but very rigorous. The results shown in Fig. 6 depict a good fit of the theoretical solution to measured data, which promotes us to discuss the physical significance behind the result.

The following issues have been validated by the result: (1) the consistency supports the conclusion that the physical framework established by this study models successfully the real process of the lateral attenuation of the scattering light measured during the Arctic winter experiment; (2) the assumptions for the point light source, the scattering to the horizontal solid angle, and the volume integral of all points are all verified to be reasonable; (3) it is also verified that the measuring approach proposed by Zhao et al. (2010) is operational and accurate to measure the attenuation of the LPL; and (4) the size of the lamp is also verified to be sufficiently large for measurements of the attenuation coefficient. The slight difference of measured and analytical results only appeared around a point where the observed ones are smooth curves but the analytical solution take a sudden turn because the two paragraphs of the analytical solution in Eq. (14) produce a transit point there. The reason is that the logarithmic relative variability rate around this point is not linear.

The physical significance of the attenuation coefficient $c(\lambda)$, and therefore the measured attenuation coefficient $\mu(\lambda)$, is perceptible from Eq. (6). The attenuation coefficient indicates the diffusion attenuation with distance as an apparent optical property of ice. The definition describes that the medium has a specific ability to attenuate the light. An adequate measuring approach is basic and important to enable the effective measurement for the attenuation ability of sea ice. The attenuation ability should be caused by the microstructure of sea ice, such as crystal size, ice density, brine volume, air inclusion, etc. It may also include the leak from both interfaces by directional scattering. The lateral attenuation ability changes with the varying salinity (Zhao et al., 2010) to point out the contribution of salt inside the sea ice to the attenuation coefficient. If salinity equals 4, the attenuation coefficient is about 2.5 m^{-1}; if salinity equals 8.5, the attenuation coefficient is about 7.5 m^{-1}.

If one wants to measure the lateral attenuation coefficient by the other size lamps or other ice conditions, the analytical solution for comparing does not need to change, just by replacing the length of lamp and the attenuation coefficient. The consistence of the analytical and measured results illustrates that the artificial light experiment is justified to be a reliable approach to measure the attenuation coefficient of LPL.

The solution from this study did not tell the connection among the extinction and the inclusions of ice theoretically. More related measurements for both lateral attenuation and the microstructure are necessary to reveal the connection in the future. The result does not also solve the net energy attenuation of the radiation, because part of the attenuated energy shifted to the vertically propagating light and we have no idea about the quantified amount of leaked light fluxes through the interfaces. An exquisitely designed experiment is expected to measure simultaneously the lateral radiation and vertical light flux through the interfaces to facilitate the calculation for net energy consume by LPL.
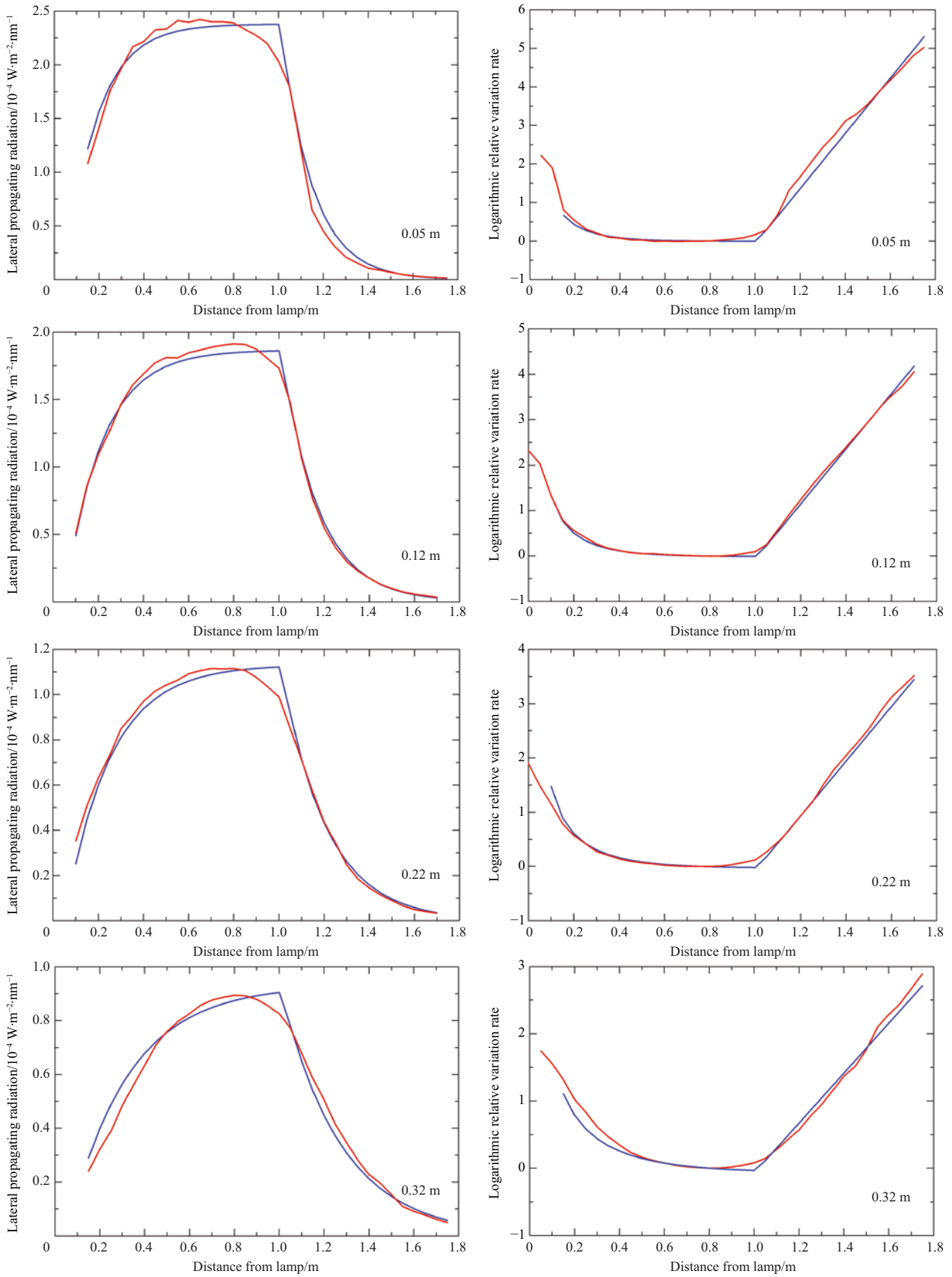
Fig. 6. The comparison of the analytical solution with the measured data of 490 nm in each level at Sta. D7. Left: lateral propagating radiation for narrow FOV; right: logarithmic relative variation rate. Red lines express observation result and blue lines are for analytical solution. From top to bottom, the depth of the PRR-810 are at 0.05, 0.12, 0.22, 0.32 m.

References

Arrigo, K R, Perovich D K, Pickart R S, et al. 2012. Massive phytoplankton blooms under Arctic sea ice. Science (Brevia), 336: 6087, doi:10.1126/science.1215065

Barber D G, Massom R A. 2007. The role of sea ice in Arctic and Antarctic Polynyas. In: Smith W O, Barber D G, eds. Polynyas: Windows to the World. Elsevier Oceanography Series, 74: 1–54

Buckley R G, Trodahl H J. 1987a. Scattering and absorption of visible light by sea ice. Nature, 326: 867–869, doi:10.1038/326867a0

Buckley R G, Trodahl H J. 1987b. Thermally driven changes in the optical properties of sea ice. Cold Regions Science and Technology, 14: 201–204

Dickson D R, Hales J V. 1963. Computation of visual range in fog and low clouds. Journal of Applied Meteorology, 2(2): 281–285

Ehn J K, Mundy C J, Barber D G. 2008a. Bio-optical and structural properties inferred from irradiance measurements within the bottommost layers in an Arctic landfast sea ice cover. J Geophys Res, 113: C03S03, doi:10.1029/2007JC004194

Ehn J K, Papakyriakou T N, Barber D G. 2008b. Inference of optical properties from radiation profiles within melting landfast sea ice. J Geophys Res, 113: C09024, doi:10.1029/2007JC004656

Gilbert G D, Schoonmaker J. 1990. Measurements of beam spread in new ice. In: Proceedings of SPIE Ocean Optics VIII, 1302: 545–555

Grenfell T C, Perovich D K. 1981. Radiation absorption coefficients of poly crystalline ice from 400–1 400 nm. J Geophys Res, 86 (C8): 7447–7450

Haines E M, Buckley R G, Trodahl H J. 1997. Determination of the depth dependent scattering coefficient in sea ice. J Geophys Res, 102(C1):1141–1151

Hanesiak J M, Barber D G, Abreu R A, et al. 2001. Local and regional albedo observations of Arctic first-year sea ice during melt ponding. J Geophys Res, 106(C1): 1005–1016

Holland M M, Bitz C M, Hunke E C, et al. 2006. Influence of the sea ice thickness distribution on polar climate in CCSM3. Journal of Climate, 19(11): 2398–2414

Light B, Maykut G A, Grenfell T C. 2004. A temperature-dependent, structural-optical model of first-year sea ice. J Geophys Res, 109, C06013, doi:10.1029/2003JC002164

Lindsay R W, Zhang J. 2005. The thinning of Arctic sea ice, 1988–2003: have we passed a tipping point?. Journal of Climate, 18(22): 4879–4894

Maffione R A, Voss J M, Mobley C D. 1998. Theory and measurements of the complete beam spread function in sea ice. Limnol Oceanogr, 43: 34–43

Maykut G, Grenfell T C. 1975. The spectral distribution of light beneath first-year sea ice in the Arctic Ocean. Limnol Oceanogr, 20(4): 554–563

Mobley C D. 1994. Light and Water: Radiative Transfer in Natural Waters. San Diego: Academic Press, 592

Mundy, C J, Gosselin M, Ehn J K,et al. 2009. Contribution of under-ice primary production to an ice-edge upwelling phytoplankton bloom in the Canadian Beaufort Sea. Geophysical Research Letters, 36: L17601, doi:10.1029/2009GL038837

Parkinson C L, Cavalieri D J, Gloersen P, et al. 1999. Arctic sea ice extents, areas and trends, 1978–1996. J Geophys Res, 104(C9): 20837–20856

Parkinson C L, Comiso J C. 2013. On the 2012 record low Arctic sea ice cover: Combined impact of preconditioning and an August storm. Geophysical Research Letters, 40(7): 1356–1361

Pegau W S, Zaneveld J R V. 2000. Field measurements of in-ice radiance. Cold Regions Science and Technology, 31: 33–46

Perovich D K. 1996. The Optical Properties of Sea Ice. US: US Army Corps of Engineers, 12–13

Perovich D K, Longacre J, Barber D G, et al. 1998. Field observations of the electromagnetic properties of first-year sea ice. Transactions on Geoscience and Remote Sensing, 36(5): 1705–1715

Rothrock D A, Yu Y, Maykut G A. 1999. Thinning of the Arctic sea-ice cover. Geophys Res Lett, 26(23): 3469–3472

Schoonmaker J S, Voss K J, Gilbert G D. 1989. Laboratory measurements of optical beams in young sea ice. Limnol Oceanogr, 34(S): 1606–1613

Trodahl H J, Buckley R G, Brown S. 1987. Diffusive transport of light in sea ice. Applied Optics 26: 3005–3011

Trodahl H J, Buckley R G, Vignaux M. 1989. Anisotropic light-radiance in and under sea ice. Cold Regions Science and Technology, 16: 305–308

Tucker W B III, Weatherly J W, Eppler D T, et al. 2001. Evidence for rapid thinning of sea ice in the western Arctic Ocean at the end of the 1980s. Geophys Res Lett, 28: 2851–2854

Voss K J, Schoonmaker J S. 1992. Temperature dependence of beam scattering in young sea ice. Applied Optics, 31: 3388–3389

Zhang Jinlun, Lindsay R, Schweiger A, et al. 2013. The impact of an intense summer cyclone on 2012 Arctic sea ice retreat. Geophysical Research Letters, 40(4): 720–726

Zhao Jinping, Barber D, Li Tao, et al. 2008. Radiation of lamp and optimized experiment using artificial light in the Arctic Ocean. Chinese Journal of Polar Science, 19(2): 249–260

Zhao Jinping, Li Tao, Barber D, et al. 2010. Attenuation of artificial lateral propagating light in winter Arctic sea ice. Cold Regions Science and Technology, 61: 6–12

Zhao Jinping, Li Tao, Zhang Shugang. 2009, The shortwave solar radiation energy absorbed by packed sea ice in the central Arctic. Advances in Earth Sciences (in Chinese), 24(1): 35–41

Zhao Jinping , Li Tao. 2010. Solar radiation penetrating through sea ice under very low solar altitude. Journal of Ocean University of China, 9(2): 116–122, doi: 10.1007/s11802-010-0116-7